

Bistability in the Electric Current through a Quantum-Dot Capacitively Coupled to a Charge-Qubit

S. M. Tabatabaei*

Department of Applied Physics, Faculty of Physics, University of Shahid Beheshti, Evin, Tehran, Islamic Republic of Iran

Received: 22 September 2017 / Revised: 21 October 2017 / Accepted: 13 November 2017

Abstract

We investigate the electronic transport through a single-level quantum-dot which is capacitively coupled to a charge-qubit. By employing the method of nonequilibrium Green's functions, we calculate the electric current through quantum dot at finite bias voltages. The Green's functions and self-energies of the system are calculated perturbatively and self-consistently to the second order of interaction between the quantum-dot and the charge-qubit by employing the Majorana fermion representation for isospin operators of the qubit. Our results show that in the particle-hole symmetric situation, the electric current of the QD exhibits a unitary linear conductance at low bias voltage and at the higher bias voltage it has a nonlinear dependence on the bias voltage. Moreover, we find that at some appropriate parameter regimes, the current through the QD as a function of gate voltage, at a fixed bias voltage shows bistability.

Keywords: Nonequilibrium green's function method; Current bistability; Perturbation theory; Majorana fermion representation of spin operators.

Introduction

A spin-degenerate single-level quantum-dot(QD) which is tunnel coupled to two metallic electrodes is the simplest model for studying electronic transport through nanostructures. The response of this model system to the external fields depends on the internal properties of the QD. In the realistic situations, such interactions like electron-electron, electron-phonon or spin-orbit interactions result in some novel static and dynamic behaviours in the system which have been the subject of many theoretical and experimental studies in the last three decades [1–15]. The most supportive motivation behind these efforts is the advancement in the engineering and fabrication of nano-scale electronic devices which could affect broad fields of interests like

nanoelectronics, spintronics, quantum computations, bioelectronics and etc.

In this work, we study the electronic transport properties of a QD in the proximity of a charge-qubit. Most of the previous works considering a similar model, have studied the decoherence of the charge-qubit or the electric current through QD by assuming the energy-gap of the charge-qubit and the coupling of the QD to the charge-qubit, to be much smaller than the electron transition rates between QD and electrodes [16–28]. In this parameter regime, the QD operate as a sensor for probing the state of the charge-qubit. However, in the opposite parameter regime, the electronic transport through the QD has not been much studied [29, 30]. In this work we are studying this parameter regime using the method of non-equilibrium Green's functions and

* Corresponding author: Tel: +982122431669; Fax: +982122431666; Email: s.m.tab90@gmail.com

the Majorana fermion representation of iso-spin operators to investigate the electric current through the QD in the steady-state at finite bias voltages. To this end, we calculate the interacting non-equilibrium Green's functions of QD and qubit self-consistently to the second order of interaction between QD and qubit. We then calculate the average occupation number of electrons, density of states and average electric current of the QD. We compare our results at the zero bias with the results obtained using the method of numerical renormalization group (NRG) [31].

The paper is organized as follows: In the next section, the model Hamiltonian and the related non-equilibrium Green's functions of the system are presented. In the results section, we present our numerical results. Finally, in the last section, we give a summary and conclusion of our work.

Materials and Methods

Our model system consists of a QD coupled to two metallic electrodes while simultaneously interacts capacitively with a charge qubit. The total Hamiltonian of the system is

$$H = H_{QD} + H_{qubit} + H_I. \quad (1)$$

The term H_{QD} is the Hamiltonian of the QD and electrodes subsystem which is given by

$$H_{QD} = \sum_{\epsilon} v_d d_{\epsilon}^{\dagger} d_{\epsilon} + \sum_{k,r,\epsilon} (v_k + \sim_r) c_{k,r,\epsilon}^{\dagger} c_{k,r,\epsilon} + t_r (c_{k,r,\epsilon}^{\dagger} d_{\epsilon} + H.c.), \quad (2)$$

where d_{ϵ}^{\dagger} and d_{ϵ} are the creation and annihilation operators of an electron with spin $\epsilon = \uparrow, \downarrow$ in the QD and v_d is the applied gate voltage. Similarly, the operators $c_{k,r,\epsilon}^{\dagger}$ and $c_{k,r,\epsilon}$ are the corresponding operators for an electron creation and annihilation with energy v_k in the left and right leads ($r = L, R$). The leads are treated as half-filled quasi-one-dimensional normal metals with chemical potentials \sim_L and \sim_R . The coupling of the QD with each lead, $t_{L,R}$, is assumed to be energy and spin independent.

The second term in Eq.(1) is the Hamiltonian of the charge qubit which is modeled as a double quantum dot which contains only one electron [32], and is described by

$$H_{qubit} = -\frac{\tilde{S}_0}{2} \dagger_3 + \frac{\Delta}{2} \dagger_1, \quad (3)$$

where \tilde{S}_0 and $\frac{\Delta}{2}$ are the energy difference and the hybridization energy between the two dots of the qubit,

respectively, and $(\dagger_1, \dagger_2, \dagger_3)$ are the usual Pauli operators describing the two dimensional Hilbert space of the qubit.

Finally, the last term in Eq.(1) describes the capacitive interaction between QD and qubit which is given by $H_I = \} n_d \dagger_3$, where n_d is the total electron number operator of QD. In addition, we take explicitly the mean-field back-action effects by adding and subtracting the operator $A = \} (\langle n_d \rangle \dagger_3 + \dagger_3 \langle n_d \rangle)$ to and from the total Hamiltonian which modifies the interaction Hamiltonian to

$$H_I = \} (n_d - \langle n_d \rangle) (\dagger_3 - \langle \dagger_3 \rangle), \quad (4)$$

and the on-site energies of the QD and qubit to $\tilde{v}_d = v_d + \} \langle \dagger_3 \rangle$ and $\tilde{S}_0 = \tilde{S}_0 - 2 \} \langle n_d \rangle$, respectively.

Before considering the nonequilibrium Green's functions of the system, we express the iso-spin operators of the qubit in terms of Majorana fermions, in order to make it possible to derive the Green's functions and self-energies using Wick's theorem. By defining three Majorana fermion operators, (y_1, y_2, y_3) , which are satisfying the usual fermionic equal-time anti-commutation relation $\{y_a, y_b\} = u_{a,b}$ and $y_a^{\dagger} = y_a$, the Majorana fermion representation of the iso-spin operators is then given by [33, 34]

$$\dagger_a = -i \delta_{abc} y_b y_c, \quad \text{for } a, b, c = 1, 2, 3, \quad (5)$$

where δ_{abc} is the Levi-Civita antisymmetric tensor.

We will determine the interacting Green's functions [35] of the QD-qubit system by taking $H_{QD} + H_{qubit}$ as the non-interacting part and H_I as the perturbing Hamiltonians. Because our Hamiltonian does not explicitly depend on time, the Green's functions are functions of time differences and it is therefore more preferable to express them in the frequency space by Fourier transformation.

The non-interacting retarded (advanced) Green's functions of the QD are defined by $g_{\epsilon\epsilon'}^{R,A}(t, t') = \mp i \epsilon (\pm t \mp t') \langle \{d_{\epsilon}(t), d_{\epsilon'}^{\dagger}(t')\} \rangle_0$, where $\langle \dots \rangle_0$ is the expectation value with respect to the ground-state of $H_{QD} + H_{DQD}$ at the zero temperature. In order to describe the correct nonequilibrium dynamics of the system, we need two other Green's functions, namely, the lesser and the greater Green's functions which are defined, respectively, by $g_{\epsilon\epsilon'}^{<}(t, t') = i \langle d_{\epsilon}^{\dagger}(t') d_{\epsilon}(t) \rangle_0$ and $g_{\epsilon\epsilon'}^{>}(t, t') = -i \langle d_{\epsilon}(t) d_{\epsilon'}^{\dagger}(t') \rangle_0$. In the frequency domain the expressions for the Green's functions $\hat{g}^{R,A}(\tilde{S})$ and

$\hat{g}^<(\check{S})$ in the matrix representation spanned by $(d_\uparrow, d_\downarrow)$ are

$$\hat{g}^R(\check{S}) = \left[\hat{g}^A(\check{S}) \right]^\dagger = \hat{I} \frac{1}{\check{S} - \tilde{V}_d + i(\Gamma_L + \Gamma_R)} \quad (6)$$

and

$$\hat{g}^<(\check{S}) = \hat{g}^R(\check{S}) \hat{\Sigma}_g^{(leads)<}(\check{S}) \hat{g}^A(\check{S}), \quad (7)$$

where \hat{I} is a 2×2 unit matrix and $\Gamma_{L,R} \equiv f |t_{L,R}|^2 \dots_0$ is the self-energy due to the coupling of QD to the leads in the standard wide-band approximation in which the density of states of the leads, \dots_0 , are assumed to be independent of energy.

Moreover, $\hat{\Sigma}_g^{(leads)<}$ is calculated using

$$\hat{\Sigma}_g^{(leads)<}(\check{S}) = 2i\hat{I} \sum_{\Gamma=L,R} \Gamma_\Gamma f_\Gamma(\check{S}), \quad (8)$$

where $f_{L,R}(\check{S}) = \dots(\sim_{L,R} - \check{S})$ and $\dots(\dots)$ is the standard Heaviside-theta function. The greater Green's function could be obtained by the relation $\hat{g}^>(\check{S}) = \hat{g}^A(\check{S}) - \hat{g}^R(\check{S}) + \hat{g}^<(\check{S})$.

For the qubit, we define its non-interacting Green's functions by $h_{mn}^{R,A}(t, t') = \mp i_n (\pm t \mp t') \langle \{y_m(t), y_n^\dagger(t')\} \rangle_0$, $h_{mn}^<(t, t') = i \langle y_m^\dagger(t') y_n(t) \rangle_0$ and $h_{mn}^>(t, t') = -i \langle y_m(t) y_n^\dagger(t') \rangle_0$. In the frequency domain and in matrix representation spanned by the basis (y_1, y_2, y_3) , the expressions for $\hat{h}^{R,A}(\check{S})$ and $\hat{h}^<(\check{S})$ are given by

$$\hat{h}^R(\check{S}) = \left[\hat{h}^A(\check{S}) \right]^\dagger = \begin{pmatrix} \check{S} + i\mathbf{U} & -i\check{S}_0 & 0 \\ i\check{S}_0 & \check{S} + i\mathbf{U} & i\Delta \\ 0 & -i\Delta & \check{S} + i\mathbf{U} \end{pmatrix}^{-1} \quad (9)$$

and

$$\hat{h}^<(\check{S}) = -2i \text{Im} \left[\hat{h}^R(\check{S}) \right] f(\check{S}), \quad (10)$$

where \mathbf{U} is an infinitesimal positive constant and $f(\check{S}) = \dots(-\check{S})$. The greater Green's function is also obtained by the relation $\hat{h}^>(\check{S}) = \hat{h}^A(\check{S}) - \hat{h}^R(\check{S}) + \hat{h}^<(\check{S})$.

To determine the interacting Green's functions of the QD and qubit we use the Dyson equations which give us the Green's functions as

$$\hat{G}^{R,A}(\check{S}) = \left[\left[\hat{g}^{R,A}(\check{S}) \right]^{-1} - \hat{\Sigma}_g^{R,A}(\check{S}) \right]^{-1}, \quad (11)$$

$$\hat{G}^<(\check{S}) = \hat{G}^R(\check{S}) (\hat{\Sigma}_g^{(leads)<} + \hat{\Sigma}_g^<)(\check{S}) \hat{G}^A(\check{S}), \quad (12)$$

$$\hat{H}^{R,A}(\check{S}) = \left[\left[\hat{h}^{R,A}(\check{S}) \right]^{-1} - \hat{\Sigma}_h^{R,A}(\check{S}) \right]^{-1} \quad (13)$$

and

$$\hat{H}^<(\check{S}) = \hat{H}^R(\check{S}) \hat{\Sigma}_h^<(\check{S}) \hat{H}^A(\check{S}), \quad (14)$$

where \hat{G} and \hat{H} represent the interacting Green's function of QD and qubit, respectively, and $\hat{\Sigma}_g$ and $\hat{\Sigma}_h$ are their corresponding selfenergies which are given in the Appendix.

Using the Green's functions of the system, various physical observables of the system could be determined. The total density of states of the QD is obtained by

$$A(\check{S}) = -\frac{1}{f} \text{Tr} [\text{Im} [\hat{G}^R(\check{S})]]. \quad (15)$$

Moreover, the expectation values of n_d and \dagger_3 could be obtained from

$$\langle n_d \rangle = -\frac{i}{2f} \int d\check{S} \text{Tr} [\hat{G}^<(\check{S})] \quad (16)$$

and

$$\langle \dagger_3 \rangle = -2 \int \frac{d\check{S}}{2f} \hat{H}_{12}^<(\check{S}). \quad (17)$$

Furthermore, the average electric current through QD in the steady-state could be calculated using

$$I = -\frac{e}{\hbar} \int \frac{d\check{S}}{2f} \Gamma_L \text{Tr} [\text{Im} [\hat{G}^<(\check{S}) + 2\hat{G}^R(\check{S}) f_L(\check{S})]]. \quad (18)$$

We see that Eqs. (11) - (14) make a closed system of equations which gives us the interacting Green's functions of QD- qubit system. However, there still remain two parameters in these equations which must be determined, the renormalized energy level and \check{S}_0 which must be calculated self-consistently in turn by the interacting Green's functions using Eqs. (16) and (17) for $\langle n_d \rangle$ and $\langle \dagger_3 \rangle$.

Results

We perform our calculations at zero-temperature and take $\Gamma = \Gamma_L + \Gamma_R$ as the unit of energy with $\hbar = e = c = 1$. Furthermore, we consider a symmetric bias voltage between two metallic leads; $\sim_L = -\sim_R = \frac{V_b}{2}$. At zero

bias, we check our results by comparing them with NRG which are obtained using "NRG LJUBLJANA"[36] package. Fig. 1 (a) shows local density of states (DOS) of the QD in the particle-hole symmetric condition, i.e $v_d = 0$ and $\dagger_3 = \check{S}_0$. The DOS exhibits central resonance peaks along with two subsequent sideband peaks with widths proportional to the Γ . The sidebands have peaks around the energies $\check{S} \approx \pm \frac{1}{2} (\Delta + \sqrt{\Delta^2 + \check{S}_0^2})$ which could be obtained

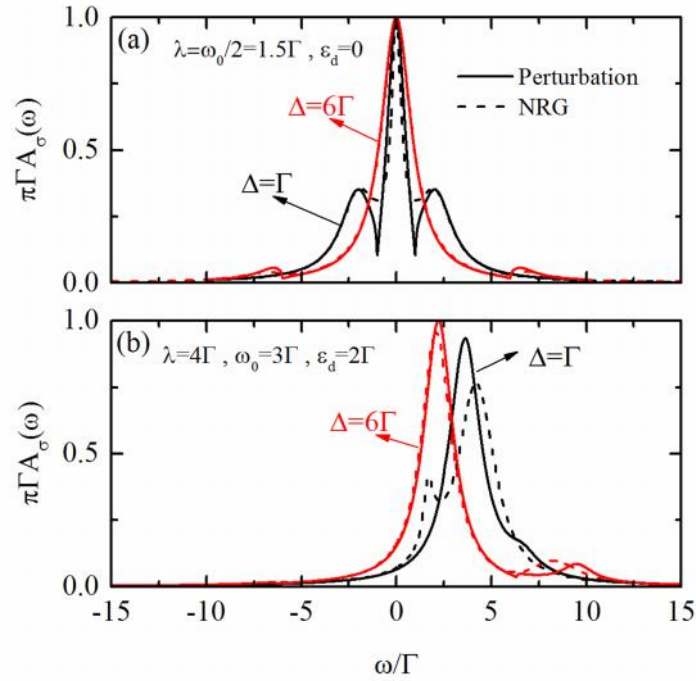


Figure 1. Single spin spectral densities of the QD calculated by perturbation method (solid lines) and NRG method (dashed lines) in zero bias voltages. For the cases (a) $V_d = 0$, $2\tilde{\xi} = \tilde{\xi}_0 = 3\Gamma$, $\Delta = \Gamma, 6\Gamma$ and (b) $V_d = 2\Gamma$, $\tilde{\xi} = \frac{2}{3}\tilde{\xi}_0 = 4\Gamma$, $\Delta = \Gamma, 6\Gamma$.

easily by calculating the single-particle excitation-energies of the isolated QD-qubit system. Furthermore, the DOS shows sharp dips exactly at $\tilde{\xi} = \pm\Delta$. The occurrence of these sharp dips are due to large values of the retarded self-energies of the QD at these points. In comparison with NRG results, we see the overall form of the density of states are in good agreement with NRG although the heights of the exterior sideband peaks and the widths of the central peaks are somehow differ from NRG. In Fig.1(b), we show the spectral densities of QD in the p-h asymmetric situations. There are only one or at most two peaks in the spectral densities. As in the p-h symmetric case, in this case, the locations and heights of the peaks in the DOS are relatively in good agreement with NRG.

Next, we study the behavior of the system in the presence of finite bias voltages. The electric current, I , and the differential conductance, $G = \frac{dI}{dV_b}$, through the QD versus bias voltage are shown in Figs. 2 (a) and (b) where the system is assumed to be in the p-h symmetric point. At zero bias voltage, the differential conductance of the QD shows its maximum value, i.e. $G = 2G_0 = \frac{2e}{h}$. By increasing the bias voltage, the differential

conductance decreases until $V_b \approx \Delta$, where a dip appears in the differential conductance and then the differential conductance shows a peak when the voltage reaches twice the energy of the sideband peaks in the spectral density, i.e. $V_b = (\Delta + \Omega)$.

In order to gain more insight about this behavior of I-V curves, we show the density of states of the QD for different voltage biases in Fig.3. For bias voltages with values $0 < V_b < 2\Delta$, the sharp dips around central peak divide into two dips with an equal distance of $\pm \frac{V_b}{2}$ around $\tilde{\xi} = \pm\Delta$. Exactly at $V_b = 2\Delta$, the two interior divided-dips reach the origin and their effect is washed out. As a result, we could expect that a dip should be formed in the differential conductance curves at $V_b = \Delta$ when the Fermi energy of the electrodes encounters the interior sharp dips in the density of states, at $\tilde{\xi} = \pm \left(|\Delta| - \frac{|V_b|}{2} \right)$. Moreover, we see in Fig. 3

that the height of the central peak is reduced when the bias voltage is increased which is responsible for the negative differential conductance for bias voltages around $V_b \approx \Delta$.

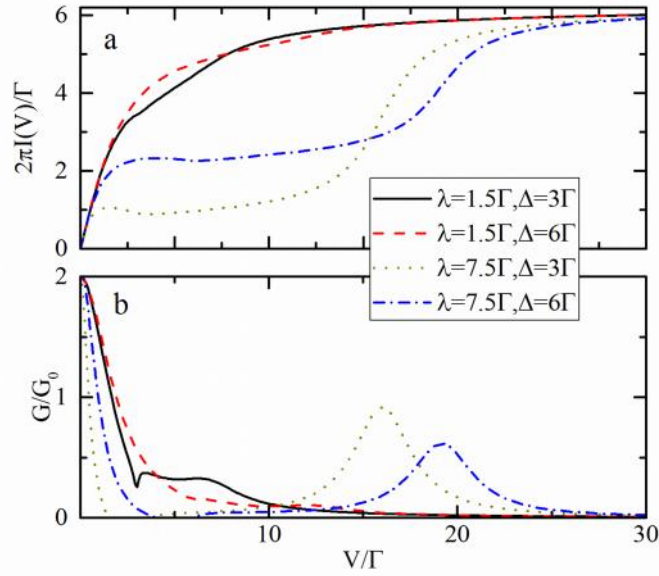


Figure 2. (a) Electric current and (b) differential conductance of the QD as a function of bias voltage for $\tilde{S}_0 = 2$, $v_d = 0$.

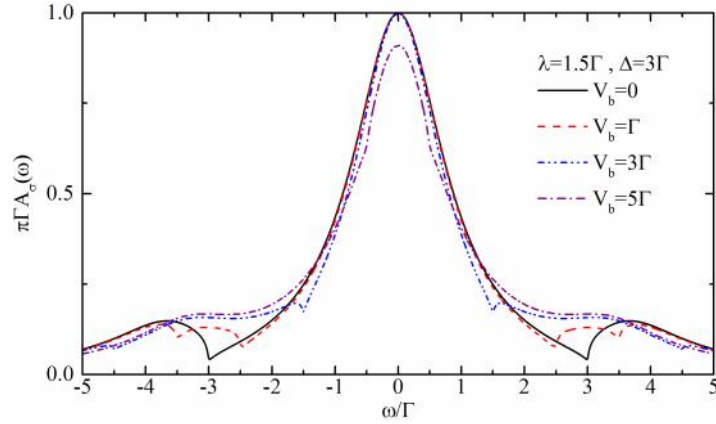


Figure 3. QD's density of states in the presence of a finite bias voltage. $\lambda = 1.5\Gamma$, $\tilde{S}_0 = 2$, $v_d = 0$, $\Delta = 3\Gamma$.

Apart from p-h symmetric point, the electric current through QD as a function of the gate voltage shows bistability. In Fig. 4, we show the electric current of the QD as a function of the gate voltage. In order to distinguish between the different stable solutions of the system, we have swept the QD's gate voltage forward and backward between values 0 to 2Γ , in the presence of a constant bias voltage. We see that the electric current through the QD in some ranges of the gate voltage shows bistability. Such bistability behavior is common features in the current characteristics of molecular junctions with an attractive electron-electron interaction [15]. Indeed, it has been shown recently [30] that the capacitive interaction of a QD with a charge qubit can induce an attractive interaction between the two electrons in the QD which would be responsible for

the appearance of the bistability behavior in the system.

Discussion

We have used the method of non-equilibrium Green's functions to study the effect of electron-electron interactions between a QD and a charge qubit. To this end, we employed the Majorana fermion representation of Pauli operators to extract the Green's functions of the system perturbatively to the second order of interaction between the QD and the charge qubit. The effect of the QD and charge qubit on each other is taken into account by calculating the self-energies and Green's functions self-consistently. We studied the spectral densities of the QD in different parameter regimes and compared our zero bias results with NRG results. We found that

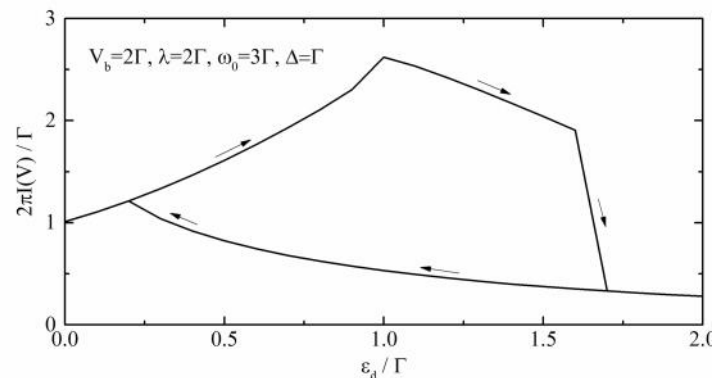


Figure 4. Electric current through QD with respect to the QD's gate voltage. $V_b = 2\Gamma$, $\lambda = 2\Gamma$, $\omega_0 = 3\Gamma$ and $\Delta = \Gamma$.

this model system could show unitary linear electric conductance in the particle-hole symmetric situations. Moreover, we have shown that in some parameter regimes the current through QD as a function of gate voltage for fixed bias exhibits bistability behavior due to the capacitive interaction with the qubit which could be of interest in the nanoelectronic devices.

References

- Schuler B, Persson M, Paavilainen S, Pavlik N, Gross L, Meyer G, Repp J. Effect of electron-phonon interaction on the formation of one-dimensional electronic states in coupled Cl vacancies. *Phys. Rev. B*, **91**(23):235443 (2015).
- Zwanenburg FA, Dzurak AS, Morello A, Simmons MY, Hollenberg LC, Klimeck G, Rogge S, Coppersmith SN, Eriksson MA. Silicon quantum electronics. *Rev. Mod. Phys.*, **85**(3):961 (2013).
- Han JE. Nonequilibrium electron transport in strongly correlated molecular junctions. *Phys. Rev. B*, **81**(11):113106 (2010).
- Laird EA, Kuemmeth F, Steele GA, Grove-Rasmussen K, Nygård J, Flensberg K, Kouwenhoven LP. Quantum transport in carbon nanotubes. *Rev. Mod. Phys.*, **87**(3):703 (2015).
- Chen SH, Chen CL, Chang CR, Mahfouzi F. Spin-charge conversion in a multiterminal Aharonov-Casher ring coupled to precessing ferromagnets: A charge-conserving Floquet nonequilibrium Green function approach. *Phys. Rev. B*, **87**(4):045402 (2013).
- Bati M, Sakiroglu S, Sokmen I. Electron transport in electrically biased inverse parabolic double-barrier structure. *Chinese Phys. B*, **25**(5):057307 (2016).
- Kornich V, Kloeffel C, Loss D. Phonon-mediated decay of singlet-triplet qubits in double quantum dots. *Phys. Rev. B*, **89**(8):085410 (2014).
- Awschalom DD, Bassett LC, Dzurak AS, Hu EL, Petta JR. Quantum spintronics: engineering and manipulating atom-like spins in semiconductors. *Science*, **339**(6124):1174-1179 (2013).
- Viennot JJ, Dartiailh MC, Cottet A, Kontos T. Coherent coupling of a single spin to microwave cavity photons. *Science*, **349**(6246):408-411 (2015).
- Prabhakar S, Melnik R, Bonilla LL. Electrical control of phonon-mediated spin relaxation rate in semiconductor quantum dots: Rashba versus Dresselhaus spin-orbit coupling. *Phys. Rev. B*, **87**(23):235202 (2013).
- Muhonen JT, Dehollain JP, Laucht A, Hudson FE, Kalra R, Sekiguchi T, Itoh KM, Jamieson DN, McCallum JC, Dzurak AS, Morello A. Storing quantum information for 30 seconds in a nanoelectronic device. *Nat. Nanotechnol.*, **9**(12):986-991 (2014).
- Bruchez M, Moronne M, Gin P, Weiss S, Alivisatos AP. Semiconductor nanocrystals as fluorescent biological labels. *Science*, **281**(5385):2013-2016 (1998).
- Li L, Wu G, Yang G, Peng J, Zhao J, Zhu JJ. Focusing on luminescent graphene quantum dots: current status and future perspectives. *Nanoscale*, **5**(10):4015-4039 (2013).
- Karwacki Ł, Trocha P, Barna J. Magnon transport through a quantum dot: Conversion to electronic spin and charge currents. *Phys. Rev. B*, **92**(23):235449 (2015).
- Eskandari-asl A. Bi-stability in single impurity Anderson model with strong electron-phonon interaction (polaron regime). *Physica B*, **497**:11-13 (2016).
- Makhlin Y, Schön G, Shnirman A. Quantum-state engineering with Josephson-junction devices. *Rev. Mod. Phys.*, **73**(2):357 (2001).
- Sprinzak D, Buks E, Heiblum M, Shtrikman H. Controlled dephasing of electrons via a phase sensitive detector. *Phys. Rev. Lett.*, **84**(25):5820 (2000).
- Makhlin Y, Schön G, Shnirman A. Statistics and noise in a quantum measurement process. *Phys. Rev. Lett.*, **85**(21):4578 (2000).
- Korotkov AN. Selective quantum evolution of a qubit state due to continuous measurement. *Phys. Rev. B*, **63**(11):115403 (2001).
- Gurvitz SA, Berman GP. Single qubit measurements with an asymmetric single-electron transistor. *Phys. Rev. B*, **72**(7):073303 (2005).
- Gurvitz SA, Mozyrsky D. Quantum mechanical approach to decoherence and relaxation generated by fluctuating environment. *Phys. Rev. B*, **77**(7):075325 (2008).
- Shnirman A, Schön G. Quantum measurements performed with a single-electron transistor. *Phys. Rev. B*,

- 57(24): 15400 (1998).
23. Mozyrsky D, Martin I, Hastings MB. Quantum-limited sensitivity of single-electron-transistor-based displacement detectors. *Phys. Rev. Lett.*, **92**(1): 018303 (2004).
 24. Oxtoby NP, Wiseman HM, Sun HB. Sensitivity and back action in charge qubit measurements by a strongly coupled single-electron transistor. *Phys. Rev. B*, **74**(4): 045328 (2006).
 25. Schulenburg J, Splettstoesser J, Governale M, Contreras-Pulido LD. Detection of the relaxation rates of an interacting quantum dot by a capacitively coupled sensor dot. *Phys. Rev. B*, **89**(19): 195305 (2014).
 26. Hell M, Wegewijs MR, DiVincenzo DP. Coherent backaction of quantum dot detectors: Qubit isospin precession. *Phys. Rev. B*, **89**(19): 195405 (2014).
 27. Hell M, Wegewijs MR, DiVincenzo DP. Qubit quantum-dot sensors: Noise cancellation by coherent backaction, initial slips, and elliptical precession. *Phys. Rev. B*, **93**(4): 045418 (2016).
 28. Tabatabaei SM. Perturbative approach to the capacitive interaction between a sensor quantum dot and a charge qubit. *Phys. Rev. B*, **95**(15): 155113 (2017).
 29. Simine L, Segal D. Electron transport in nanoscale junctions with local anharmonic modes. *J. Chem. Phys.*, **141**(1): 014704 (2014).
 30. Hamo A, Benyamini A, Shapir I, Khivrich I, Weissman J, Kaasbjerg K, Oreg Y, von Oppen F, Ilani S. Electron attraction mediated by coulomb repulsion. *Nature*, **535**(7612):395-400 (2016).
 31. Bulla R., Costi T. and Pruschke T. Numerical renormalization group method for quantum impurity systems. *Rev. Mod. Phys.*, **80**(2): 395 (2008).
 32. Liu YY, Petersson KD, Stehlik J, Taylor JM, Petta JR. Photon emission from a cavity-coupled double quantum dot. *Phys. Rev. Lett.*, **113**(3): 036801 (2014).
 33. Schad P, Shnirman A, Makhlin Y. Using Majorana spin-1/2 representation for the spin-boson model. *Phys. Rev. B*, **93**(17): 174420 (2016).
 34. Schad P, Makhlin Y, Narozhny BN, Schön G, Shnirman A. Majorana representation for dissipative spin systems. *Ann. Phys.*, **361**: 401-422 (2015).
 35. Stefanucci G. and van Leeuwen R. Nonequilibrium Many-Body Theory of Quantum Systems: A Modern Introduction, *Camb. Univ. Press* (2013).
 36. Zitko R. The package is available at <http://nrgljubljana.ijs.si>.

Appendix: Selfenergies of QD and qubit subsystems

The QD's second order self-energies are[28]

$$\hat{\Sigma}_g^R(\check{S}) = \int \int \frac{d\check{S}_1}{2f} [\hat{g}^<(\check{S})\Phi^R(\check{S}-\check{S}_1) + \hat{g}^R(\check{S})\Phi^<(\check{S}-\check{S}_1) + \hat{g}^R(\check{S})\Phi^R(\check{S}-\check{S}_1)] \quad (\text{A.1})$$

and

$$\hat{\Sigma}_g^<(\check{S}) = \int \int \frac{d\check{S}_1}{2f} \hat{g}^<(\check{S})\Phi^<(\check{S}-\check{S}_1), \quad (\text{A.2})$$

where

$$\Phi^R(\check{S}) = \int \frac{d\check{S}_1}{2f} [h_{11}^<(\check{S}+\check{S}_1)h_{22}^A(\check{S}_1) + h_{11}^R(\check{S}+\check{S}_1)h_{22}^<(\check{S}_1) - h_{12}^<(\check{S}+\check{S}_1)h_{21}^A(\check{S}_1) - h_{12}^R(\check{S}+\check{S}_1)h_{21}^<(\check{S}_1)] \quad (\text{A.3})$$

and

$$\Phi^<(\check{S}) = \int \frac{d\check{S}_1}{2f} [h_{11}^<(\check{S}+\check{S}_1)h_{22}^>(\check{S}_1) - h_{12}^<(\check{S}+\check{S}_1)h_{21}^>(\check{S}_1)]. \quad (\text{A.4})$$

For the qubit, the second order self-energies are

$$\hat{\Sigma}_h^{R,<}(\check{S}) = \begin{pmatrix} F_{22}^{R,<}(\check{S}) & F_{21}^{R,<}(\check{S}) & 0 \\ F_{12}^{R,<}(\check{S}) & F_{11}^{R,<}(\check{S}) & 0 \\ 0 & 0 & 0 \end{pmatrix}, \quad (\text{A.5})$$

where

$$F_{mn}^R(\check{S}) = \int \sum_{\epsilon=\uparrow,\downarrow} \int \frac{d\check{S}_1}{2f} [h_{mn}^<(\check{S})\Pi_\epsilon^R(\check{S}-\check{S}_1) + h_{mn}^R(\check{S})\Pi_\epsilon^<(\check{S}-\check{S}_1) + h_{mn}^R(\check{S})\Pi_\epsilon^R(\check{S}-\check{S}_1)] \quad (\text{A.6})$$

and

$$F_{mn}^<(\check{S}) = \int \sum_{\epsilon=\uparrow,\downarrow} \int \frac{d\check{S}_1}{2f} h_{mn}^<(\check{S})\Pi_\epsilon^<(\check{S}-\check{S}_1). \quad (\text{A.7})$$

The functions $\Pi_\epsilon^{R,<}(\check{S})$, in the above equations, are given by

$$\Pi_\epsilon^R(\check{S}) = \int \frac{d\check{S}_1}{2f} [g_{\epsilon\epsilon}^<(\check{S}+\check{S}_1)g_{\epsilon\epsilon}^A(\check{S}_1) + g_{\epsilon\epsilon}^R(\check{S}+\check{S}_1)g_{\epsilon\epsilon}^<(\check{S}_1)] \quad (\text{A.8})$$

And $\Pi_\epsilon^<(\check{S}) = \int \frac{d\check{S}_1}{2f} g_{\epsilon\epsilon}^<(\check{S}+\check{S}_1)g_{\epsilon\epsilon}^>(\check{S}_1). \quad (\text{A.9})$